Figure 3. High-resolution genome-wide mRNA expression and CpG methylation profiling. GenomeStudio view of mRNA-seq data and CpG methylation map of the genomic region spanning the *Nespas-Gnas* maternally imprinted locus. (*Top*) Genomic stacked alignment plots of wild-type oocytes, *Dnmt3L$^{-/-}$* oocytes, and sperm. (*Middle*) Open boxes and black line plots represent the location of CGIs and the distribution of CpG densities of individual CpGs, respectively. (*Bottom*) Red, purple, blue, and green dots represent the methylation levels at individual CpGs in wild-type oocyte, *Dnmt3L$^{-/-}$* oocyte, sperm, and blastocyst genomes, respectively. The red shaded areas show the extent of two maternal imprinting control regions (ICRs).
doi:10.1371/journal.pgen.1002440.g003

Dnmt3L$^{-/-}$ oocytes was observed (Figure 5B, 5C). These results suggested that changes in gene expression did not occur during oogenesis, despite global intragenic hypomethylation in *Dnmt3L$^{-/-}$* oocytes. Furthermore, the expression levels and exon patterns of maternally-methylated imprinted genes across each ICR were

not altered in *Dnmt3L$^{-/-}$* oocytes (Figure 3 and Figure 5D). This result suggested that the disruption of maternal methylation imprints in the *Dnmt3L$^{-/-}$* oocyte genome was not due to the lack of their transcription [36]. On the other hand, maternal methylation imprints at ICRs (and many other hypermethyla-

Table 2. CpG methylation profiling of 12 maternal and 3 paternal imprinting control regions.

	Gene locus	Chr.	Extents of the ICRs†		Average methylation levels				
			Start	End	Wild-type oocyte	DnmtLⁱ⁻/⁻ oocyte	Sperm	Blastocyst	ESC
Maternally methylate imprinted genes	Nespas-Gnas	2	174,119,863	174,126,564	99.3%	5.6%	3.9%	38.2%	55.9%
	Gnas (exon1A)	2	174,150,877	174,154,638	95.2%	3.5%	4.1%	20.4%	7.8%
	Peg10	6	4,696,743	4,699,483	95.9%	6.7%	5.5%	31.8%	57.1%
	Mest	6	30,684,932	30,689,966	96.5%	2.3%	4.2%	30.7%	52.6%
	Peg3	7	6,679,787	6,684,257	98.1%	3.0%	2.5%	32.1%	42.8%
	Snrpn	7	67,147,381	67,151,583	94.1%	35.7%	4.6%	34.3%	64.9%
	Kcnq1ot1	7	150,480,736	150,482,810	97.9%	2.2%	4.3%	34.1%	52.0%
	Plagl1	10	12,809,697	12,812,131	99.9%	1.3%	7.4%	35.4%	53.0%
	Grb10	11	11,925,127	11,927,100	98.0%	1.2%	5.3%	38.5%	78.7%
	Zrsr1	11	22,871,610	22,874,212	94.1%	5.2%	6.8%	34.8%	47.0%
	Igf2r	17	12,934,169	12,935,816	99.1%	0.9%	3.8%	44.2%	53.2%
	Impact	18	13,130,435	13,133,510	97.2%	2.4%	6.6%	43.1%	38.6%
Paternally methylated imprinted genes	H19	7	149,764,673	149,771,930	13.5%	0.6%	96.5%	40.8%	65.5%
	Rasgrf1	9	89,767,090	89,775,128	7.4%	0.7%	92.0%	25.2%	59.4%
	Dlk1-Meg3	12	110,762,703	110,773,093	18.9%	0.9%	96.8%	32.4%	83.1%

†: The extents of each region in germ cells were determined by bisulfite sequencing study [39].
doi:10.1371/journal.pgen.1002440.t002

tions at transcribed regions) in wild-type oocyte genomes might be the result of gene transcription via *Dnmt3L*-mediated intragenic methylation.

Surprisingly, gene expression in ESC genomes was negatively correlated with promoter methylation and was not positively correlated with gene-body methylation (Figure S12). Meanwhile, these ESCs showed the apparent expression of all DNA methyltransferase gene families including *Dnmt3L* (Figure S13). Previous studies indicated that the zygotic and somatic functioning of *Dnmt3L* is not essential for global methylation in ESCs in mice [6]. Thus, unlike oocytes, the functional role of *Dnmt3L* in gene-body methylation after fertilization is unclear. However, the expression of pluripotency-associated genes, *Pou5f1*, *Klf4*, *Sox2*, *Myc*, *Nanog*, and *Lin28a*, was clearly observed in ESCs. The expression of *Pou5f1*, *Lin28a*, and *Glis1*, recently identified as maternal reprogramming factors, were also observed in oocytes (Figure S14). While differential expression of the pluripotency genes among germ and stem cells was observed, the promoter regions of these genes demonstrated low-level methylation in almost all of the examined cells. In sperm cells, only the *Nanog* promoter was hypermethylated (this result was similar to a previous study [29]).

Identification and characterization of germline differentially methylated regions

To identify gDMRs, the average CpG methylation levels of individual CpG islands (CGIs), which are CpG-rich genomic regions often lacking DNA methylation, were calculated. Recently, Illingworth et al. determined the number of CGIs by deep sequencing of isolated, unmethylated DNA clusters [37]. Among the 23,021 mouse CGIs (22,974 CGIs were informative in both oocytes and sperm), 2014 were highly methylated (≥80% methylation) in oocytes, 818 were highly methylated in sperm, and 377 were highly methylated in both germ cells (Figure 6A). Furthermore, we also identified 1678 gDMRs (≥80% methylation

in 1 gamete and ≤20% in the other), 1329 of which were oocyte-specific methylated CGIs, while the remaining 349 were sperm-specific methylated CGIs (Figure 6A, Figure S6, and Table S2). Among these gDMRs, 646 gDMRs were confirmed to show a differential methylation status between GV oocytes and sperm (by similar criteria: ≥75% methylation in 1 gamete and ≤25% in the other); the methylation status was previously examined by performing large-scale bisulfite sequencing of CpG-rich regions of the genome (reduced representation bisulfite sequencing: RRBS) (Table S3) [38]. Additionally, almost all known ICRs except *Zdbf2* DMRs (which do not have any CGIs) were re-identified from our gDMR list (Table S2).

A total of 78% oocyte-methylated gDMRs (n = 1045) were located within the intragenic regions. Approximately 25% of the oocyte-methylated gDMRs (n = 322) overlap with either the first exon or the proximal promoter regions of the genes, as has been observed with most of the described maternal ICRs [39]; only 5% of the sperm-methylated gDMR (n = 18) showed such overlap. Alternatively, 34% of sperm-methylated gDMRs (n = 120) overlap with intergenic regions, as in all known paternal ICRs (Figure 6B). Interestingly, oocyte-methylated gDMRs in transcribed regions tended to be more abundant within highly expressed genes, but such a trend was not observed in the sperm genome (Figure 6C). Oocyte-methylated gDMRs were also identified in non-imprinted genes, such as the DNA methyltransferase genes (*e.g.*, *Dnmt1* and *Dnmt3b*) and some male germline-specific genes (*e.g.*, *Piwil1*, *Spag1*, *Ggnbp2*, *Tbpl1*, *Spata16*, *Ggn*, *Acrbp*, and *Cd46*). The oocyte-methylated gDMR in *Dnmt1* was located in spermatocyte- and somatic-specific exons, while oocyte-specific exons were hypomethylated in oocytes (Figure S9). *Dnmt3L*⁻/⁻ oocytes also showed hypomethylation in most of these gDMRs. Significant changes in the expression levels of genes with alternative splicing patterns were not observed in the *Dnmt3L*⁻/⁻ oocyte genome (Figure 3, Figure 5E, and Figure S9). These results indicate that these oocyte-specific methylated gDMRs do not regulate gene expression or alternative splicing during the oocyte stage.
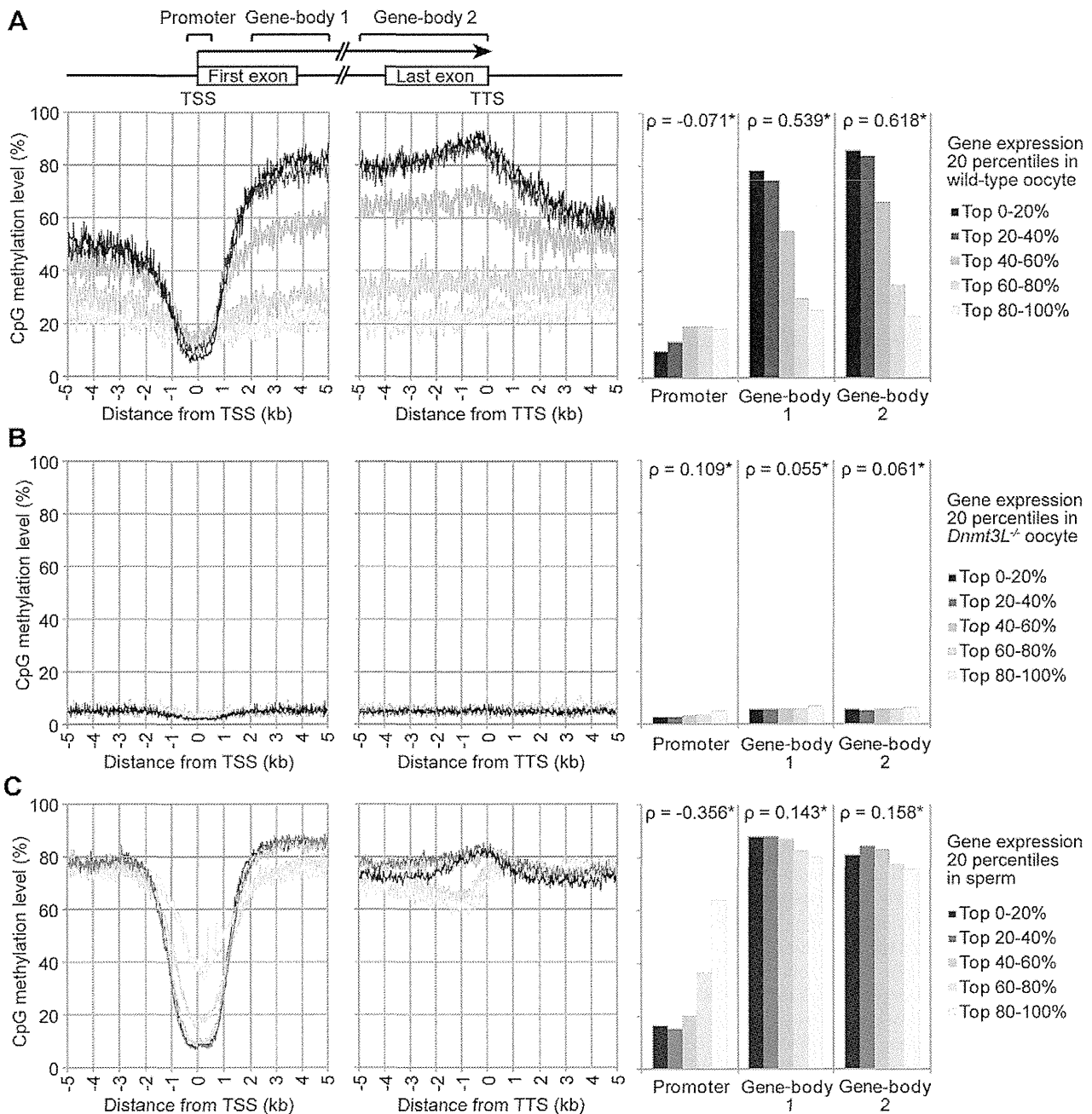
— 124 —

Figure 4. Relationship between gene expression and methylation in promoter and gene-body regions in mouse germ cells. The expression level of genes in wild-type oocytes (A), sperm (B), and Dnmt3L$^{-/-}$ oocytes (C) were divided into 5 percentile groups. The distribution of methylation is shown ±5 kb from the transcription termination site (TTS; left) and transcription start site (TSS; middle). The graphs on the right show the average methylation levels in the promoter and gene-body regions. Spearman's rank correlation coefficient (ρ) was used to test the statistical significance of the correlation between gene expression and DNA methylation levels (*: p<1×10^{-9}).
doi:10.1371/journal.pgen.1002440.g004

To determine whether or not these germ cell-specific methylations are maintained after fertilization, when the genomes undergo global demethylation, the individual CGI methylation levels in blastocyst genomes were calculated. In blastocysts, all ICRs demonstrated low to moderate methylation (25.1–64.3%), whereas many gDMRs were demethylated (0–20%) (Figure 6D). Furthermore, 817 oocyte-methylated gDMRs (including Piwil1, despite being a non-imprinted gene locus) and 34 sperm-specific gDMRs were resistant to demethylation during early embryogenesis (≥20% methylation in blastocysts) (Figure 6D and Table S2).

Among the demethylation-resistant gDMRs, a novel gDMR in the intron of Gpr1 (Figure S10) was found to be a tissue-specific, paternally-expressed imprinted gene [40]. Bisulfite sequencing analysis showed that this gDMR was hypomethylated in Dnmt3L$^{-/-}$ oocytes and maternal allele-specific methylation was detected in this region in blastocysts (Figure 6E). Methylation profiles in ESCs showed that 26% (n = 213) of the demethylation-resistant gDMRs became less methylated (0–20%) whereas the other gDMRs maintained or increased DNA methylation (Figure S15). Among ICRs, only Gnas exon1A ICR was demethylated (7.8%),
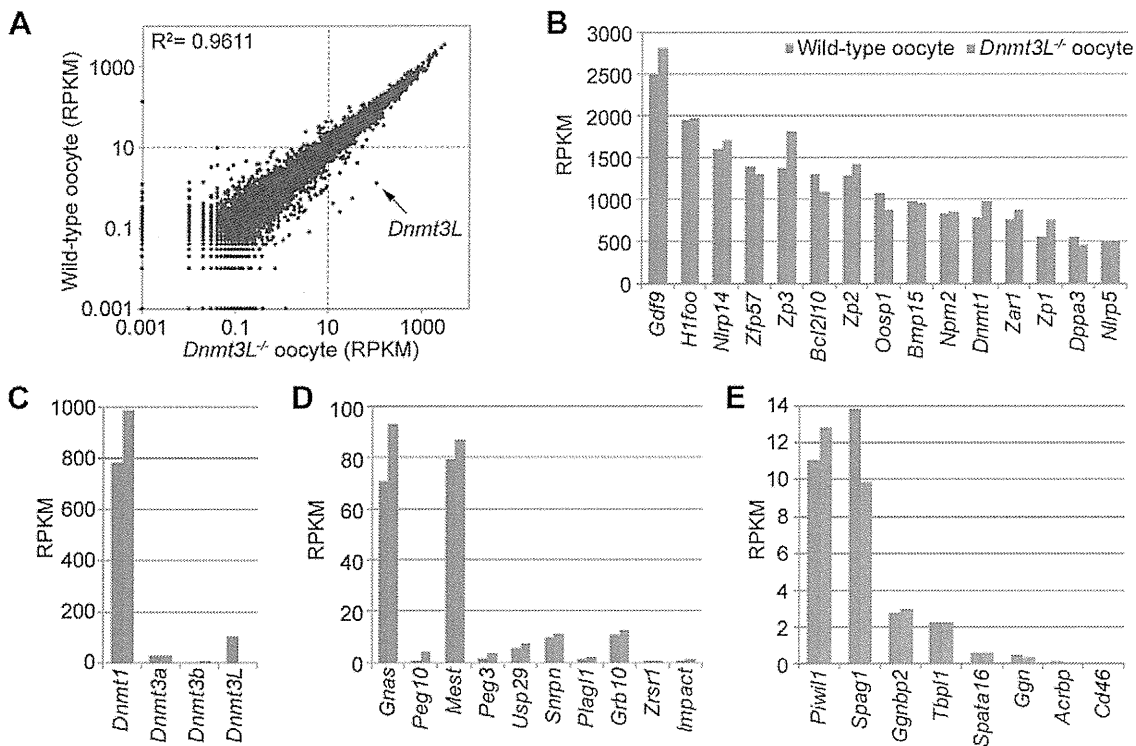
Figure 5. Comparison of gene expression profiles between wild-type and $Dnmt3L^{-/-}$ oocytes. (A) Scatter plot and correlation coefficient (R^2) of RPKM values of 20,854 genes in wild-type and $Dnmt3L^{-/-}$ oocytes. Expression levels of oocyte-specific genes (B), DNA methyltransferase genes (C), maternally-imprinted genes that are potentially necessary to establish methylation imprints (D), and male germline-specific genes that contain oocyte-specific methylated CpG islands (CGIs) (E).
doi:10.1371/journal.pgen.1002440.g005

whereas the other ICRs developed partial or high methylation levels (range, 38.6–83.1%) in ESCs (Table 2). Among other demethylation-sensitive gDMRs, which were demethylated (<20% methylation) in blastocysts, many (76%, n = 264) sperm-methylated gDMRs were re-methylated (≥20% methylation); most (81%, n = 416) of the oocyte-methylated gDMRs maintained low methylation (0–20%) in ESCs (Figure S15). Finally, out of 704 demethylation-resistant (in blastocysts) oocyte-methylated gDMRs which were informative in $Dnmt3L^{-/-}$ oocytes, only 4 remained hypermethylated (80–100% methylation) in the $Dnmt3L^{-/-}$ oocyte genome. However, almost all other oocyte-specific methylation marks at gDMRs were $Dnmt3L$-dependent (Figure 6F). These results suggest that $Dnmt3L$-mediated methylation during oogenesis regulates the establishment of most heritable oocyte-specific marks, including genomic imprints.

Discussion

To the best of our knowledge, this is the first study to generate single-base resolution maps of DNA methylomes spanning the entire genome of mouse germ cells. The oocyte maps are particularly valuable and informative because, in the past, such an analysis was prohibitive due to the need for large quantities of DNA. Recently, Smallwood et al. [38] reported large-scale DNA methylation patterns in mouse germ cells by using the RRBS method, which targets only CpG-rich regions. However, our more comprehensive results provide strong evidence that gene expression was positively correlated to $Dnmt3L$-dependent intragenic methylation in oocytes, and that methylation patterns in oocytes differed from those in sperm and non-germline cells.

The functional role of gene-body methylation has been an enigma despite its conservation in plants and animals [41–43]. Maunakea et al. [44] suggested that gene-body methylation is involved in the regulation of alternative splicing events. Although methylated gDMRs were detected in the alternative exons of $Dnmt1$ and $Gnas$ in mouse oocytes, loss of oocyte-specific methylation marks in the $Dnmt3L^{-/-}$ oocytes did not affect the expression patterns of alternatively spliced transcripts. Therefore, our results indicate that gene-body methylation is not involved in alternative splicing in oocytes.

Previously, Chotalia et al. [36] showed that transcription during the oocyte stage is required for the establishment of maternal methylation marks on an imprinted gene. The present results show that $Dnmt3L^{-/-}$ oocytes lost almost all of their maternal methylation imprints while maintaining a constant amount of mRNA through each ICR despite the global loss of intragenic methylation. Thus, these results strongly suggest that the establishment of genomic imprints via transcription is mediated by $Dnmt3L$-dependent intragenic methylation.

A possible mechanism for gene-body methylation involves the exposure of intragenic regions to DNA methyltransferases, considering that RNA polymerase disrupts the chromatin structure during transcription. However, not all transcripts across gDMRs corresponded to highly expressed genes in oocytes (Figure 6C). Therefore, other epigenetic marks with an open chromatin structure might also be important for DNA methylation in oocytes. For instance, a recent knockout study showed that $Kdm1b$, which encodes histone H3K4 demethylase, is required for the establishment of some maternal methylation imprints [45]. Thus, several factors, including transcriptional and epigenetic modifica-
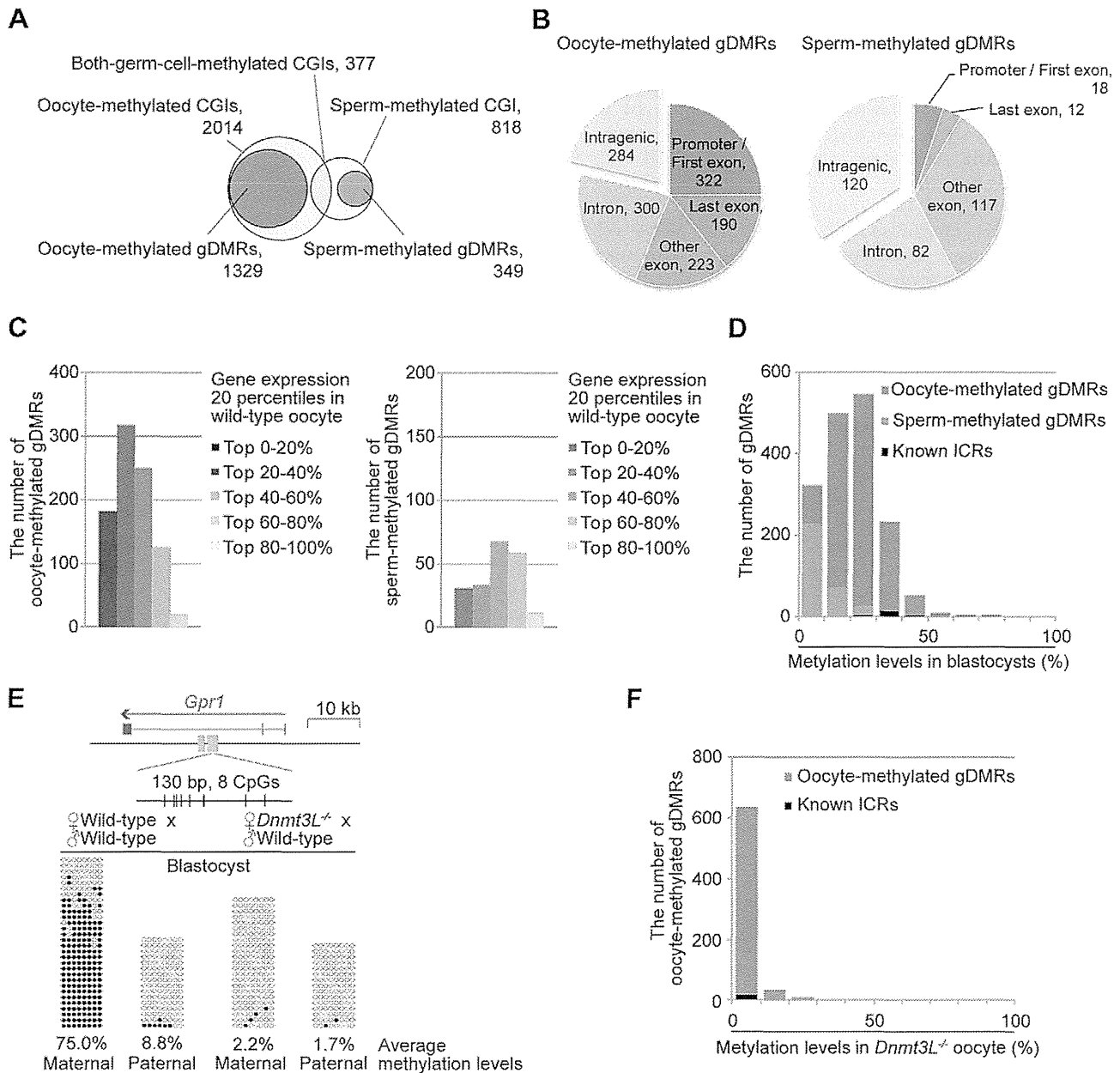
— 126 —

A

Both-germ-cell-methylated CGIs, 377

Oocyte-methylated CGIs, 2014

Sperm-methylated CGI, 818

Oocyte-methylated gDMRs, 1329

Sperm-methylated gDMRs, 349

B

Oocyte-methylated gDMRs   Sperm-methylated gDMRs

Promoter / First exon, 18

Last exon, 12

Intragenic, 284

Promoter / First exon, 322

Intron, 300

Last exon, 190

Other exon, 223

Intragenic, 120

Other exon, 117

Intron, 82

C

Gene expression 20 percentiles in wild-type oocyte
- Top 0-20%
- Top 20-40%
- Top 40-60%
- Top 60-80%
- Top 80-100%

Gene expression 20 percentiles in wild-type oocyte
- Top 0-20%
- Top 20-40%
- Top 40-60%
- Top 60-80%
- Top 80-100%

D

- Oocyte-methylated gDMRs
- Sperm-methylated gDMRs
- Known ICRs

Metylation levels in blastocysts (%)

E

Gpr1   10 kb

130 bp, 8 CpGs

♀Wild-type x ♂Wild-type   ♀Dnmt3L⁻/⁻ x ♂Wild-type

Blastocyst

75.0% Maternal   8.8% Paternal   2.2% Maternal   1.7% Paternal   Average methylation levels

F

- Oocyte-methylated gDMRs
- Known ICRs

Metylation levels in Dnmt3L⁻/⁻ oocyte (%)

Figure 6. Identification of germline differentially methylated CGIs from DNA methylome profiles. (A) Venn-like diagram of two groups of CGIs, namely, oocyte-methylated CGIs (light pink) and sperm-methylated CGIs (light blue) and two groups of gDMRs, namely, oocyte-methylated gDMRs (red) and sperm-methylated gDMRs (blue). (B) The genomic distribution of 1329 oocyte-methylated (left) and 349 sperm-methylated gDMRs (right). The gDMRs were classified into 5 genomic locations; promoter (within 500-bp upstream from the first exon) or first exon, last exon, other exon, intron, and intergenic region. (C) The locations of the intragenic 1045 oocyte-methylated (left) and 229 sperm-methylated gDMRs (right). The gDMRs were classified into 5 gene group locations; the genes were divided into 5 percentile groups according to their expression levels in wild-type oocytes and sperm, as shown in Figure 3. (D) Histograms of the methylation levels of the gDMRs in blastocysts. The number of newly identified oocyte-specific, sperm-specific methylated gDMRs, and known ICRs are shown in black, red, and blue, respectively. (E) Bisulfite sequencing at the Gpr1 gDMR in mouse blastocysts. (Top) Schematic representation of paternally-expressed Gpr1. The gene and gDMRs are shown in blue and green, respectively, and CpG sites are represented by vertical bars. (Bottom) Methylated and unmethylated CpGs are indicated by open and closed circles, respectively. The maternal and paternal alleles were distinguished by three polymorphisms between C57BL/6N and JF1 mice (G/A at 63,247,064; T/A at 63,247,072; and TA/AG at 63,247,089–63,247,090 on chromosome 1). (F) Histograms of the methylation levels of the demethylation-resistant oocyte-methylated gDMRs in Dnmt3L⁻/⁻ oocytes. The number of newly identified oocyte-specific, sperm-specific methylated gDMRs, and known ICRs are shown in black, red, and blue, respectively.
doi:10.1371/journal.pgen.1002440.g006

tions, might be involved in Dnmt3L-mediated intragenic methylation.

The results of this study show that gene-body methylation was correlated to gene expression in sperm. However, the extent of

that correlation is much less than in oocytes due to genome-wide hypermethylation, including in low-CpG-density regions. In male germline cells, global methylation acquisition begins during late embryonic development and before birth [3]. To more clearly

— 127 —

show this correlation, analysis of early-stage germ cells in fetal or neonatal animals might be required. Surprisingly, a positive correlation between mRNA expression and gene-body methylation was not observed in mouse ESCs. In addition, the accumulation of non-CpG methylation was not observed in mouse ESCs. These results contradict the results of another study, which showed that active transcription was associated with intragenic DNA methylation with non-CpG methylation in human ESCs [22,23]. This discrepancy might reflect the differences between human and mouse ESCs, the precise cell derivations or culture conditions [46,47]. However, further comparative studies on germ cell epigenomes from other species are required to further elucidate the functional role of epigenetic marking systems.

In this study, a large number of heritable oocyte-specific methylation marks were identified within a set of novel CpG islands [37]. The difference in the number of oocyte- and sperm-specific gDMRs reflects the fact that only 3 or 4 paternally-methylated imprinted loci were observed, as compared to approximately 20 maternally-methylated imprinted loci. The reason for the relative abundance of oocyte-specific methylated CGIs might be related to the intragenic methylation of CpG-rich regions, which are hypomethylated in sperm. The results show that most of the oocyte-specific marks are *Dnmt3L*-dependent, similar to results recently obtained by RRBS-based analysis [38]. However, whether all of these CpG-rich regions serve as imprinting methylation marks is unclear. For instance, although many genes with oocyte-specific methylation marks were identified (Figure 6B), the evidence that these genes were imprinted was lacking (*e.g.*, *Piwil1* and *Dnmt1*). These methylation marks might not be involved in the formation of a fertile oocyte but might play crucial roles in gene expression after fertilization. Furthermore, ESC methylomes showed that many gDMRs, especially sperm-specific gDMRs, acquired new methylation patterns after implantation. Methylation of these CGIs might control tissue-specific gene expression [48,49]. Partial alternation of imprinted methylation patterns in ESCs were observed in the present study, potentially caused by significant differences in the extent of the ICRs during embryo development [39]. A fuller understanding of epigenetic stability will require further methylome profiling during early embryogenesis and stem cell differentiation. The present study also identified a gDMR as a novel ICR candidate in the intron of the imprinted *Gpr1* gene. Thus, traditional promoter arrays may not identify all ICRs. However, further analyses are needed to determine which gDMRs, identified in the CpG methylome maps, are true ICRs at the imprinted *Gpr1-Zdbf2* locus [40,50].

mRNA-seq results showed that the expression levels of most genes in the wild-type and $Dnmt3L^{-/-}$ oocytes were similar. For instance, the expression level of almost all oocyte-specific genes, which regulate ovarian follicle formation, reproduction, and early development, were not significantly altered (Figure 5B and Table S1). These results are consistent with the findings of previous studies, which showed that $Dnmt3L^{-/-}$ female mice were capable of producing fertile oocytes (however, their offspring were not viable due to the lack of imprinting) [5,6]. Thus, regulation of oocyte-specific genes must be beyond the control of *Dnmt3L*-dependent cytosine methylation.

Although $Dnmt3L^{-/-}$ oocytes showed global hypomethylation at low to high CpG densities, some families of retrotransposons, such as LINEs and LTRs, were partially methylated at moderate to high CpG densities. Therefore, *Dnmt3L*-independent methylation might be involved in the silencing of retrotransposons and completion of oocyte meiosis. Previously, De La Fuente et al. [51]

showed that *Hells* (also known as *Lsh*), which encodes a member of the sucrose non-fermenter 2 (SNF2) family of chromatin remodeling proteins, is required for DNA methylation of IAP and pericentromeric satellite repeats as well as repression of IAP retrotransposition in pachytene oocytes. Unfortunately, measurement of the methylation levels of satellite DNA, which is abundant in the pericentromeric regions, was not possible because these sequences were excluded from our analysis. However, a previous sequencing study showed that methylation levels of satellite DNA did not differ between the wild-type and $Dnmt3L^{-/-}$ oocytes [52]. Combined, these results suggest the presence of 2 types of oocyte methylation patterns: (i) *Dnmt3L*-mediated intragenic methylation that is essential for early embryogenesis and (ii) *Dnmt3L*-independent retroviral and pericentromeric methylation, which may be mediated by *Hells* activity, is crucial for oocyte meiosis [51]. Further studies on *Hells*-mediated oocyte methylation are required to elucidate the details of this mechanism.

Previous studies on the cytosine methylation of mtDNA have been highly controversial. A recent study by Shock et al. [53] reported cytosine methylation and hydroxymethylation in mammalian mitochondria. Our results indicated that mtDNA is unmethylated in blastocysts and ESCs, but is partially methylated in germ cells. Whether or not 5-hydroxymethylcytosine (5-hmC) exists in mitochondrial or genomic chromosomes of germ cells remains unclear. Meanwhile, rapid hydroxylation of 5-methylcytosine (5-mC) in the paternal pronucleus during zygotic development was also recently reported [54,55]. Currently, it is difficult to assess hydroxymethylation profiles in oocyte genomes due to the limited DNA recovery. Further investigation of cytosine modification during germ cell and zygote development will be required in the future to better understand this process.

The DNA methylome maps of mouse germ cells, in this study, were derived from SBS data and, therefore, accurately represent methylation levels of individual CpGs on a whole-genome level. The adaptation of the SBS method for small-scale DNA analysis, described in the present report, has the potential to enable further analyses of germline lineages. The current work examined SBS library construction using 3 methods, MethylC-seq, WBA-seq, and PBAT. MethylC-seq basically required only micrograms of DNA [22,23,56], thus over amplification might cause redundancy in oocyte libraries. The latter methods allow comprehensive methylome analysis in samples with low amounts of starting DNA by avoiding DNA damage due to sodium bisulfite treatment (after adapter ligation, in the case of MethylC-Seq). Recent studies using BS sequencing have shown that methylated cytosine is abundant in the non-CpG regions of human pluripotent stem cells and mouse oocytes [22,23,39,56]; however, the function of non-CpG methylation in mammalian genomes remains unclear. The PBAT results also showed an abundance of non-CpG methylation in oocytes, with results similar to a previous sequencing study on imprinted loci [39]. However, accurate assessment of non-CpG methylation is required using increased sequencing depths because methylation levels of the non-CpG sites were much lower than those of the CpG sites. SBS library construction was conducted by WBA-seq from 2000 fully matured (metaphase II stage) oocytes; sufficient quantities for sequencing were not obtained. During oogenesis, most of the oocyte specific imprinted methylation marks were established during the GV stage. This contrasted to a previous study where a continuous increase in methylation levels was observed [38]. Further improvement of SBS methods, requiring smaller amounts of DNA, is needed to provide complete germ cell methylome maps and to elucidate the exact function of non-CpG methylation in germ cells.

In conclusion, we constructed the first extensive, high-resolution maps of DNA methylomes of mouse oocytes and sperm. These maps described the epigenetic properties of these DNA methylomes. Our data could serve as a platform for future studies to elucidate the role of epigenetic modifications in the development and functioning of germ and stem cells. Such studies are anticipated to improve our understanding of epigenetic reprogramming.

Materials and Methods

Preparation of MethylC-seq libraries

Five thousand germinal vesicle (GV)-stage oocytes were collected from the ovarian follicles of adult (7- to 9-week-old) female C57BL/6N mice (Clea Japan, Tokyo, Japan) 44–48 h after they were injected with equine chorionic gonadotropin. Three hundred blastocysts at embryonic day 3.5 were obtained from superovulated adult female C57BL/6N mice by flushing the uterus. Genomic DNA was extracted using the QIAamp DNA Mini Kit (Qiagen, Valencia, CA). Sperm were released from the cauda epididymises of adult male C57BL/6N mice. Sperm DNA was isolated by a standard phenol-chloroform extraction procedure with dithiothreitol (DTT). Genomic DNA from 2 lines of ESCs derived from C57BL/6J mice (Clea Japan) was extracted using the DNeasy Blood & Tissue Kit (Qiagen). DNA samples were sheared into 100-bp fragments in oocytes and 200-bp fragments in other samples using the Covaris S2 focused acoustic system (Covaris, Woburn, MA). Cytosine-methylated adapters (Illumina, San Diego, CA) were ligated to DNA by using the Paired-End DNA Sample Prep Kit or ChIP-Seq DNA Sample Prep Kit (Illumina). DNA fragments were isolated by 2–3% agarose gel electrophoresis and purified using the QIAquick Gel Extraction Kit (Qiagen). Sodium bisulfite conversion was performed using the Epitect Bisulfite Kit (Qiagen).

All bisulfite-converted DNA molecules were polymerase chain reaction (PCR)-amplified as follows: 2.5 U of Hot Start Taq polymerase (TaKaRa, Tokyo, Japan), 5 μL 10× PCR buffer, 25 μM dNTPs, 1 μL of each PCR Primer PE 1.0 and 2.0 (Illumina) (50 μL final). Thermocycling parameters were: initial denaturation at 94°C for 1 min, 15–25 cycles of denaturation at 94°C for 30 s, annealing at 65°C for 30 s, and extension at 72°C for 30 s, followed by a final extension at 72°C for 5 min. PCR reaction products were purified using the QIAquick kit (Qiagen).

Preparation of whole WBA-seq libraries

Two thousand GV-stage oocytes were collected from 7- to 9-week-old female C57BL/6N mice (Clea Japan) and, 2300 GV-stage oocytes were collected from 7–15-week-old $Dnmt3L^{-/-}$ female mice (129SvJae×C57BL/6N hybrid genetic background) [6,57]. Genomic DNA was extracted using the QIAamp DNA Mini Kit (Qiagen), and then bisulfite-treated with Epitect Bisulfite Kit (Qiagen). Subsequently, the bisulfite-converted DNA was amplified using Epitect Whole Bisulfitome Kit (Qiagen). The collected DNA was sheared into 200-bp fragments using Covaris S2. Unmodified Paired-End adapters (Illumina) were ligated to the DNA by using the Paired-End DNA Sample Prep Kit (Illumina). DNA fragments were isolated by 2% agarose gel electrophoresis and purified using the QIAquick Kit (Qiagen). All DNA was PCR amplified and purified in the same manner as the MethylC-seq method, except the number of PCR cycles was reduced to 7.

Preparation of PBAT libraries

GV-stage oocytes (400) and blastocysts (100) were obtained from 7- to 9-week-old female C57BL/6N mice (Clea Japan), and genomic DNA was extracted using the QIAamp DNA Mini Kit (Qiagen). The isolated oocyte and blastocyst genomic DNA and 100 ng of genomic DNA from sperm, blastocysts, and ESCs containing 1:200 amount of unmethylated lambda DNA (Invitrogen, Carlsbad, CA) were bisulfite-treated using the MethylCode Bisulfite Conversion Kit (Invitrogen). Details of the PBAT method are unpublished [Miura F & Ito T, personal communication]. Briefly, bisulfite-treated DNA were double-stranded using Klenow Fragments (3'- 5' exo-) (New England Biolabs, Ipswich, MA) with random primers containing 5' biotin tags and Illumina PE adaptors. The biotinylated molecules (first strand) were captured using Dynabeads M280 Streptavidin (Invitrogen) and double-stranded using Klenow Fragments (3'-5' exo-) with random primers containing Illumina PE adaptors (second strand). Finally, template DNA strands were synthesized as complementary DNA with a second strand (unmethylated C is converted to T) using Phusion Hot Start High-Fidelity DNA Polymerase (New England Biolabs) with PCR Primer PE 1.0 (Illumina).

Preparation of mRNA sequencing libraries

Total RNA from 1000 wild-type GV oocytes, 500 $Dnmt3L^{-/-}$ GV oocytes, sperm, and ESCs was extracted using the RNeasy Mini Kit (Qiagen) and treated with DNase I (Promega, Madison, WI). RNA-Seq libraries were constructed using the mRNA-Seq Sample Preparation Kit (Illumina).

Sequencing

The MethylC-seq for blastocysts, WBA-seq, and PBAT libraries were sequenced on a HiSeq 2000 sequencing system (Illumina); the other MethylC-seq and mRNA-seq libraries were sequenced on a Genome Analyzer II (Illumina). Sample preparation, cluster generation, and sequencing were performed using the Paired-End Cluster Generation Kit-HS and the TruSeq SBS Kit-HS for the HiSeq 2000. Similarly, the Paired-End Cluster Generation Kits v2 and v4 and 18- and 36-Cycle Sequencing Kits v3 and v4 were used for the Genome Analyzer II. All kits were from Illumina.

Gene mapping

All sequenced reads were processed using the standard Illumina base-calling pipeline (v1.4–1.7). Generated sequence tags were mapped onto the mouse genome (mm9, UCSC Genome Browser, July 2007, Build 37.1) by using the Illumina ELAND program.

MethylC-seq tags (36 or 76 nt) were mapped with a custom Perl program, as described previously [17,22]. Briefly, all cytosines in the tags were replaced by thymines. Next, these tags were aligned to 2 mouse genome reference sequences (mm9), such that the antisense strand had cytosines replaced by thymines and the sense strand had guanines replaced by adenines. Finally, all tags (32–76 nt) that mapped uniquely without any mismatches to both strands were compiled and used for further analyses.

The 76 nt WBA-seq tags were mapped as follows. All tags were converted to 2 types of reads; in 1 read ("For" read), cytosines were replaced by thymines and in the other read ("Rev" read), guanines were replaced by adenines. Both "For" and "Rev" reads were aligned to sense and antisense mm9 strands. A total of 793, 397, 948, 480, and 238 million tags were aligned in wild-type oocytes, $Dnmt3L^{-/-}$ oocytes, sperm, blastocysts, and ESC genomes, respectively. To avoid bias, tags mapped with multiple hits or matched chromosome M (mitochondria), chromosome Y, or 3 types of repetitive sequences (simple repeat, low complexity repeat, and satellite DNA sequences) were omitted from further analyses.

The 47 nt PBAT tags (trimmed first 4 nt and last 1 nt) were mapped as follows. All guanidines in the tags were replaced by

— 129 —

adenines, and these tags were aligned to sense and antisense strands mm9.

For gene-level analysis, the concentrations of the perfectly matching 35 nt (trimmed first nt) mRNA-seq tags from wild-type oocytes, $Dnmt3L^{-/-}$ oocytes, sperm, and ESCs were calculated for the genomic regions corresponding to those covered by the RefSeq transcript models. The expression level of 20,854 unique genes was ranked by expression levels (calculated as RPKM values) in each library (Table S1). A total of 33, 28, 23, and 25 tags were aligned in 4 mRNA-seq libraries, respectively. mRNA-seq data analysis was performed and visualized using GenomeStudio Data Analysis software (Illumina).

Methylation analysis

The percentage of individual cytosines methylated at all CpG sites covered by at least 1 read was calculated as 100×(number of aligned cytosines (methylated cytosines))/(total number of aligned cytosines and thymines (originally unmethylated cytosines)). All genomic CpG methylation data are available on our website (http://www.nodai-genome.org/mouse_en.html). The CpG and non-CpG (CpH) methylation levels determined by PBAT results were calculated as the ratio between the total read C and the total read T mapped to genomic cytosines. Bisulfite conversion failure rates were calculated by read C:T ratios from lambda DNA mapping data. The failure rates were as follows: GV oocyte, 0.009; sperm, 0.008; blastocysts, 0.011; and ESCs, 0.006. Locations of transposable elements in the mouse genome (mm9) were obtained from the UCSC Genome Browser, and the average methylation levels of the whole genome and each transposable element were recalculated from the ratio of the aligned cytosines and thymines in each sequence. Lists of 23,021 CGIs were obtained from a previous report [37]. Around the TSS and TTS (±5 kb), genomic regions were divided into 20-bp bins. For each bin, the average methylation value was calculated for each gene. The expression level of 20,854 genes was divided into 5 percentile groups ranked by RPKM values, and the average methylation level for each group was mapped onto the gene structure model. These computational analyses were performed using a custom Perl program. Supercomputing resources were provided by the Human Genome Center, Institute of Medical Science, University of Tokyo.

Statistical analysis

Correlations between gene expression ranks and average methylation levels in the promoter (±500 bp from the TTS) or gene-body regions (gene-body 1: +2 to +5 kb from the TSS; gene-body 2: 0 to −5 kb from the TTS) were calculated using Spearman's rank correlation coefficient (ρ). An R-squared value (R^2) was calculated to evaluate the correlation of RPKM values between wild-type and $Dnmt3L^{-/-}$ oocytes. Statistical analysis was performed using the R statistical package.

Bisulfite sequencing

To analyze the methylation of the three transposable elements (L1 LINE, B1/Alu SINE, and IAP LTR), 20 wild-type GV oocytes were obtained from adult female C57BL/6N mice. Bisulfite sequencing conditions and primer sets for the three transposable elements were described, previously [52]. To analyze the methylation of the $Gpr1$ locus, 10 blastocysts were obtained from BJF1 (C57BL/6N×JF1) and $Dnmt3L^{mat-/-}$ ($Dnmt3L^{-/-}$ ×JF1) mice [6,57]. Genomic DNA from blastocysts was isolated using the QIAamp DNA Mini Kit (Qiagen) and treated with sodium bisulfite with the Epitect Bisulfite Kit (Qiagen). The $Gpr1$ gDMR sequence was amplified with 2 rounds of nested PCR. The

first-round PCR reaction contained 1 U of Hot Start Taq polymerase (TaKaRa), 1× PCR buffer, 200 μM dNTPs, 1 μM forward primer, and 1 μM reverse primer (20 μL final). Thermo-cycling parameters were as follows: initial denaturation at 94°C for 1 min, 35 cycles of denaturation at 94°C for 30 s, annealing at 50°C for 30 s, and extension at 72°C for 30 s, followed by a final extension at 72°C for 5 min. Subsequently, 2 μL of the product was used as the input for the second-round PCR, which was performed in the same manner. Primer sets for the nested PCR were as follows: Gpr1-BSF1 (5′-GATTAGATTAGGTTAG-TTTGGAA-3′) and Gpr1-BSR1 (5′-ACTAAAACACTAAT-CACCAAATA-3′) for the first round; Gpr1-BSF2 (5′-AGAT-TAGGTTAGTTTGGAATT-3′) and Gpr1-BSR2 (5′-AACAC-TAATCACCAAATAATTC-3′) for the second round. The second-round PCR product was subcloned and sequenced, as described previously [50]. The percentage methylation was calculated as 100×(number of methylated CpG dinucleotides)/ (total number of CpGs). At least 10 clones from each parental allele were sequenced. Sequence data were analyzed using the QUMA quantification tool for methylation analysis [58].

Accession number

The MethylC-seq, WBA-seq, PBAT, and mRNA-seq data in this study have been deposited in the DNA Data Bank of Japan (DDBJ) under accession number DRA000484.

Supporting Information

Figure S1 Schematic of the SBS library construction procedure. MethylC-Seq libraries were generated by ligation of methylated sequencing adapters to fragmented genomic DNA followed by gel purification, sodium bisulfite conversion, and PCR amplification (*left*). WBA-seq libraries were generated by ligation of unmodified sequencing adapters to bisulfite-modified (amplified using EpiTect Whole Bisulfitome Kits) and fragmented genomic DNA followed by gel purification and PCR amplification (*middle*). PBAT libraries were generated by double-stranded DNA synthesis from bisulfite-treated (single-stranded) DNA with random primers containing sequencing adapters (*right*).
(TIF)

Figure S2 The percent of the oocyte and sperm genomes covered by differing minimum numbers of MethylC-seq and WBA-seq reads.
(TIF)

Figure S3 Sequencing bias towards mitochondrial and repetitive DNA sequences. (A) Average read depths for autosomal chromosomes and chromosome M (mitochondria) of mouse oocyte and sperm genomes. Occupancy of transposable elements in reads from SBS libraries before (B) and after (C) filtering the biased reads. (D) Genomic CpG coverage of SBS reads for each chromosome of mouse oocyte (orange: MethylC-seq, red: combined between MethylC-seq and WBA-seq) and sperm genomes (blue).
(TIF)

Figure S4 Average CpG methylation levels in genomic chromosomal DNA and mitochondrial DNA.
(TIF)

Figure S5 High-resolution DNA methylome map on mouse X inactivation center region in chromosome X (100,200,000–101,200,000). GenomeStudio view of Refseq's positions, repetitive element, CpG methylation map, CpG densities, CGI positions, and CGI methylation map were shown. Red, purple, blue, green,

— 130 —

and khaki dots and boxes represent the methylation levels at individual CpGs and CGIs in wild-type oocyte, $Dnmt3L^{-/-}$ oocyte, sperm, blastocyst, and ESC genomes, respectively, as shown in Figure 1.
(TIF)

Figure S6 DNA methylome maps of each chromosome of mouse germ cells. The methylation levels of each chromosome in wild-type oocytes, $Dnmt3L^{-/-}$ oocytes, and sperm in 10 kb windows (excluding mitochondrial chromosome, chromosome Y, and unplaced contigs). Red, purple, and blue lines represent the methylation levels in wild-type oocytes, $Dnmt3L^{-/-}$ oocytes, and sperm, respectively. Red and blue boxes represent oocyte-methylated and sperm-methylated gDMRs, and red and blue pins indicate maternal and maternal ICRs, respectively.
(TIF)

Figure S7 Methylation profiling of transposable elements in mouse germ cells. (A) CpG methylation levels are plotted as a function of CpG densities for L1 LINE, B1/Alu SINE, and LTR/ERVK retrotransposons (approximately 10% of the latter are intracisternal A particle (IAP) LTRs). Data for high CpG densities including less than 100 genomic CpGs were not plotted. (B) Bisulfite sequencing of L1 LINE, B1/Alu SINE, and IAP LTR retrotransposons. Methylated and unmethylated CpGs are indicated by open and closed circles, respectively.
(TIF)

Figure S8 Transcriptome and DNA methylome profiling at *H19-Igf2*, GenomeStudio view of mRNA-seq data (*top*) and CpG methylation map (*bottom*) of the genomic region spanning each locus. The blue shaded areas show the extent of the paternally-methylated gDMR.
(TIF)

Figure S9 Transcriptome and DNA methylome profiling at *Dnmt1*. The red shaded areas show the extent of the maternally-methylated gDMR.
(TIF)

Figure S10 Transcriptome and DNA methylome profiling at *Gpr1-Zdbf2*. The blue and red shaded areas show the extent of the paternally- and maternally-methylated gDMRs, respectively.
(TIF)

Figure S11 Quantification of the ratio of methylated (total number of read C) versus unmethylated cytosines (total number of read T) by PBAT results. Bar charts represent cytosine methylation ratio (A) at CpG (*left*), CpHpG (*middle*), and CpHpH (*right*) contexts and bisulfite-conversion failure rate (B) calculated by C:T ratio from lambda DNA mapping data. Total number of mapped reads is shown on these charts (*Top*).
(TIF)

Figure S12 Relationship between gene expression and intragenic methylation in ESCs. (A) The expression level of genes in ESCs was divided into 5 percentile groups. The distribution of methylation is shown ±5 kb from the transcription termination site (TTS; *left*) and transcription start site (TSS; *middle*). The graphs on the right show the average methylation levels in the promoter and gene-body regions. Spearman's rank correlation coefficient (ρ) was used to test the statistical significance of the correlation between gene expression and DNA methylation levels (*: $p < 1 \times 10^{-9}$).
(TIF)

Figure S13 Expression profiles of DNA methyltransferase gene families. Red, purple, blue, and khaki bars represent RPKM values of individual genes in wild-type oocytes, $Dnmt3L^{-/-}$ oocytes, sperm, and ESCs.
(TIF)

Figure S14 Expression profiles of pluripotency-associated genes among wild-type oocytes, $Dnmt3L^{-/-}$ oocytes, sperm, and ESCs.
(TIF)

Figure S15 Histograms of the methylation levels of the demethylation-resistant (*left*) and demethylation-sensitive gDMRs (*right*) in ESCs. The number of oocyte-specific and sperm-specific methylated gDMRs is shown in red and blue, respectively.
(TIF)

Table S1 Gene transcript profiling for germ cells, blastocysts, and embryonic stem cells by mRNA-seq.
(XLSX)

Table S2 DNA methylation profiles of 23,021 CGIs.
(XLSX)

Table S3 Average DNA methylation profiles of 646 gDMRs determined by SBS and RRBS methods.
(XLSX)

Acknowledgments

Author Contributions

Conceived and designed the experiments: H Kobayashi, Y Suzuki, T Kono. Performed the experiments: H Kobayashi, T Sakurai. Analyzed the data: H Kobayashi, M Imai, Y Suzuki. Contributed reagents/materials/analysis tools: H Kobayashi, T Sakurai, M Imai, N Takahashi, A Fukuda, O Yayoi, S Sato, K Nakabayashi, K Hata, Y Sotomaru, Y Suzuki. Wrote the paper: H Kobayashi, T Kono.

References

1. Li E (2002) Chromatin modification and epigenetic reprogramming in mammalian development. Nat Rev Genet 3: 662–673.
2. Jaenisch R, Bird A (2003) Epigenetic regulation of gene expression: how the genome integrates intrinsic and environmental signals. Nat Genet 33 Suppl: 245–254.
3. Lees-Murdock DJ, Walsh CP (2008) DNA methylation reprogramming in the germ line. Epigenetics 3: 5–13.
4. Sasaki H, Matsui Y (2008) Epigenetic events in mammalian germ-cell development: reprogramming and beyond. Nat Rev Genet 9: 129–140.
5. Bourc'his D, Xu GL, Lin CS, Bollman B, Bestor TH (2001) Dnmt3L and the establishment of maternal genomic imprints. Science 294: 2536–2539.
6. Hata K, Okano M, Lei H, Li E (2002) Dnmt3L cooperates with the Dnmt3 family of de novo DNA methyltransferases to establish maternal imprints in mice. Development 129: 1983–1993.
7. Kaneda M, Okano M, Hata K, Sado T, Tsujimoto N, et al. (2004) Essential role for de novo DNA methyltransferase Dnmt3a in paternal and maternal imprinting. Nature 429: 900–903.
8. Kono T, Obata Y, Wu Q, Niwa K, Ono Y, et al. (2004) Birth of parthenogenetic mice that can develop to adulthood. Nature 428: 860–864.
9. Hirasawa R, Chiba H, Kaneda M, Tajima S, Li E, et al. (2008) Maternal and zygotic Dnmt1 are necessary and sufficient for the maintenance of DNA methylation imprints during preimplantation development. Genes Dev 22: 1607–1616.
10. Bourc'his D, Bestor TH (2004) Meiotic catastrophe and retrotransposon reactivation in male germ cells lacking Dnmt3L. Nature 431: 96–99.
11. Webster KE, O'Bryan MK, Fletcher S, Crewther PE, Aapola U, et al. (2005) Meiotic and epigenetic defects in Dnmt3L-knockout mouse spermatogenesis. Proc Natl Acad Sci U S A 102: 4068–4073.

— 131 —

12. Hata K, Kusumi M, Yokomine T, Li E, Sasaki H (2006) Meiotic and epigenetic aberrations in Dnmt3L-deficient male germ cells. Mol Reprod Dev 73: 116–122.

13. Shoji M, Tanaka T, Hosokawa M, Reuter M, Stark A, et al. (2009) The TDRD9-MIWI2 complex is essential for piRNA-mediated retrotransposon silencing in the mouse male germline. Dev Cell 17: 775–787.

14. Kuramochi-Miyagawa S, Watanabe T, Gotoh K, Takamatsu K, Chuma S, et al. (2010) MVH in piRNA processing and gene silencing of retrotransposons. Genes Dev 24: 887–892.

15. Cokus SJ, Feng S, Zhang X, Chen Z, Merriman B, et al. (2008) Shotgun bisulphite sequencing of the Arabidopsis genome reveals DNA methylation patterning. Nature 452: 215–219.

16. Down TA, Rakyan VK, Turner DJ, Flicek P, Li H, et al. (2008) A Bayesian deconvolution strategy for immunoprecipitation-based DNA methylome analysis. Nat Biotechnol 26: 779–785.

17. Lister R, O'Malley RC, Tonti-Filippini J, Gregory BD, Berry CC, et al. (2008) Highly integrated single-base resolution maps of the epigenome in Arabidopsis. Cell 133: 523–536.

18. Meissner A, Mikkelsen TS, Gu H, Wernig M, Hanna J, et al. (2008) Genome-scale DNA methylation maps of pluripotent and differentiated cells. Nature 454: 766–770.

19. Ball MP, Li JB, Gao Y, Lee JH, LeProust EM, et al. (2009) Targeted and genome-scale strategies reveal gene-body methylation signatures in human cells. Nat Biotechnol 27: 361–368.

20. Brunner AL, Johnson DS, Kim SW, Valouev A, Reddy TE, et al. (2009) Distinct DNA methylation patterns characterize differentiated human embryonic stem cells and developing human fetal liver. Genome Res 19: 1044–1056.

21. Deng J, Shoemaker R, Xie B, Gore A, LeProust EM, et al. (2009) Targeted bisulfite sequencing reveals changes in DNA methylation associated with nuclear reprogramming. Nat Biotechnol 27: 353–360.

22. Lister R, Pelizzola M, Dowen RH, Hawkins RD, Hon G, et al. (2009) Human DNA methylomes at base resolution show widespread epigenomic differences. Nature 462: 315–322.

23. Laurent L, Wong E, Li G, Huynh T, Tsirigos A, et al. (2010) Dynamic changes in the human methylome during differentiation. Genome Res 20: 320–331.

24. Popp C, Dean W, Feng S, Cokus SJ, Andrews S, et al. (2010) Genome-wide erasure of DNA methylation in mouse primordial germ cells is affected by AID deficiency. Nature 463: 1101–1105.

25. Serre D, Lee BH, Ting AH (2010) MBD-isolated Genome Sequencing provides a high-throughput and comprehensive survey of DNA methylation in the human genome. Nucleic Acids Res 38: 391–399.

26. Li Y, Zhu J, Tian G, Li N, Li Q, et al. (2010) The DNA methylome of human peripheral blood mononuclear cells. PLoS Biol 8: e1000533. doi:10.1371/journal.pbio.1000533.

27. Gu H, Bock C, Mikkelsen TS, Jager N, Smith ZD, et al. (2010) Genome-scale DNA methylation mapping of clinical samples at single-nucleotide resolution. Nat Methods 7: 133–136.

28. Howlett SK, Reik W (1991) Methylation levels of maternal and paternal genomes during preimplantation development. Development 113: 119–127.

29. Farthing CR, Ficz G, Ng RK, Chan CF, Andrews S, et al. (2008) Global mapping of DNA methylation in mouse promoters reveals epigenetic reprogramming of pluripotency genes. PLoS Genet 4: e1000116. doi:10.1371/journal.pgen.1000116.

30. Barhanin J, Lesage F, Guillemare E, Fink M, Lazdunski M, et al. (1996) K(V)LQT1 and lsK (minK) proteins associate to form the I(Ks) cardiac potassium current. Nature 384: 78–80.

31. Shin J, Bossenz M, Chung Y, Ma H, Byron M, et al. (2010) Maternal Rnf12/RLIM is required for imprinted X-chromosome inactivation in mice. Nature 467: 977–981.

32. Weber M, Hellmann I, Stadler MB, Ramos L, Paabo S, et al. (2007) Distribution, silencing potential and evolutionary impact of promoter DNA methylation in the human genome. Nat Genet 39: 457–466.

33. Edwards JR, O'Donnell AH, Rollins RA, Peckham HE, Lee C, et al. (2010) Chromatin and sequence features that define the fine and gross structure of genomic methylation patterns. Genome Res 20: 972–980.

34. Arnaud P, Hata K, Kaneda M, Li E, Sasaki H, et al. (2006) Stochastic imprinting in the progeny of Dnmt3L−/− females. Hum Mol Genet 15: 589–598.

35. Minami N, Tsukamoto S (2006) Role of oocyte-specific genes in the development of mammalian embryos. Reproductive Medicine and Biology 5: 175–182.

36. Chotalia M, Smallwood SA, Ruf N, Dawson C, Lucifero D, et al. (2009) Transcription is required for establishment of germline methylation marks at imprinted genes. Genes Dev 23: 105–117.

37. Illingworth RS, Gruenewald-Schneider U, Webb S, Kerr ARW, James KD, et al. (2010) Orphan CpG Islands Identify Numerous Conserved Promoters in the Mammalian Genome. PLoS Genet 6: e1001134. doi:10.1371/journal.ppat.1001134.

38. Smallwood SA, Tomizawa SI, Krueger F, Ruf N, Carli N, et al. (2011) Dynamic CpG island methylation landscape in oocytes and preimplantation embryos. Nat Genet 43: 811–814.

39. Tomizawa S, Kobayashi H, Watanabe T, Andrews S, Hata K, et al. (2011) Dynamic stage-specific changes in imprinted differentially methylated regions during early mammalian development and prevalence of non-CpG methylation in oocytes. Development 138: 811–820.

40. Hiura H, Sugawara A, Ogawa H, John RM, Miyauchi N, et al. (2010) A tripartite paternally methylated region within the Gpr1-Zdbf2 imprinted domain on mouse chromosome 1 identified by meDIP-on-chip. Nucleic Acids Res 38: 4929–4945.

41. Hellman A, Chess A (2007) Gene body-specific methylation on the active X chromosome. Science 315: 1141–1143.

42. Feng S, Cokus SJ, Zhang X, Chen PY, Bostick M, et al. (2010) Conservation and divergence of methylation patterning in plants and animals. Proc Natl Acad Sci U S A 107: 8689–8694.

43. Zemach A, McDaniel IE, Silva P, Zilberman D (2010) Genome-wide evolutionary analysis of eukaryotic DNA methylation. Science 328: 916–919.

44. Maunakea AK, Nagarajan RP, Bilenky M, Ballinger TJ, D'Souza C, et al. (2010) Conserved role of intragenic DNA methylation in regulating alternative promoters. Nature 466: 253–257.

45. Ciccone DN, Su H, Hevi S, Gay F, Lei H, et al. (2009) KDM1B is a histone H3K4 demethylase required to establish maternal genomic imprints. Nature 461: 415–418.

46. Ginis I, Luo Y, Miura T, Thies S, Brandenberger R, et al. (2004) Differences between human and mouse embryonic stem cells. Dev Biol 269: 360–380.

47. Tesar PJ, Chenoweth JG, Brook FA, Davies TJ, Evans EP, et al. (2007) New cell lines from mouse epiblast share defining features with human embryonic stem cells. Nature 448: 196–199.

48. Song F, Smith JF, Kimura MT, Morrow AD, Matsuyama T, et al. (2005) Association of tissue-specific differentially methylated regions (TDMs) with differential gene expression. Proc Natl Acad Sci U S A 102: 3336–3341.

49. Shiota K, Kogo Y, Ohgane J, Imamura T, Urano A, et al. (2002) Epigenetic marks by DNA methylation specific to stem, germ and somatic cells in mice. Genes Cells 7: 961–969.

50. Kobayashi H, Yamada K, Morita S, Hiura H, Fukuda A, et al. (2009) Identification of the mouse paternally expressed imprinted gene Zdbf2 on chromosome 1 and its imprinted human homolog ZDBF2 on chromosome 2. Genomics 93: 461–472.

51. De La Fuente R, Baumann C, Fan T, Schmidtmann A, Dobrinski I, et al. (2006) Lsh is required for meiotic chromosome synapsis and retrotransposon silencing in female germ cells. Nat Cell Biol 8: 1448–1454.

52. Kaneda M, Hirasawa R, Chiba H, Okano M, Li E, et al. (2010) Genetic evidence for Dnmt3a-dependent imprinting during oocyte growth obtained by conditional knockout with Zp3-Cre and complete exclusion of Dnmt3b by chimera formation. Genes to Cells 15: 169–179.

53. Shock LS, Thakkar PV, Peterson EJ, Moran RG, Taylor SM (2011) DNA methyltransferase 1, cytosine methylation, and cytosine hydroxymethylation in mammalian mitochondria. Proc Natl Acad Sci U S A 108: 3630–3635.

54. Iqbal K, Jin SG, Pfeifer GP, Szabo PE (2011) Reprogramming of the paternal genome upon fertilization involves genome-wide oxidation of 5-methylcytosine. Proc Natl Acad Sci U S A 108: 3642–3647.

55. Wossidlo M, Nakamura T, Lepikhov K, Marques CJ, Zakhartchenko V, et al. (2011) 5-Hydroxymethylcytosine in the mammalian zygote is linked with epigenetic reprogramming. Nat Commun 2: 241.

56. Lister R, Pelizzola M, Kida YS, Hawkins RD, Nery JR, et al. (2011) Hotspots of aberrant epigenomic reprogramming in human induced pluripotent stem cells. Nature 471: 68–73.

57. Koide T, Moriwaki K, Uchida K, Mita A, Sagai T, et al. (1998) A new inbred strain JF1 established from Japanese fancy mouse carrying the classic piebald allele. Mamm Genome 9: 15–19.

58. Kumaki Y, Oda M, Okano M (2008) QUMA: quantification tool for methylation analysis. Nucleic Acids Res 36: W170–175.

— 132 —